Ballistic charge transport in graphene and light propagation in periodic dielectric structures with metamaterials: A comparative study

Yury P. Bliokh,[1,2] Valentin Freilikher,[1,3] and Franco Nori[1,4]

[1]*CEMS, RIKEN, Saitama, 351-0198, Japan*
[2]*Department of Physics, Technion-Israel Institute of Technology, Haifa 32000, Israel*
[3]*Department of Physics, Jack and Pearl Resnick Institute, Bar-Ilan University, Israel*
[4]*Department of Physics, University of Michigan, Ann Arbor, Michigan 48109-1040, USA*

We explore the optical properties of periodic layered media containing left-handed metamaterials. This study is based on several analogies between the propagation of light in metamaterials and charge transport in graphene. We derive the conditions when these two problems become equivalent, i.e., the equations and the boundary conditions for the corresponding wave functions coincide. We show that the photonic band-gap structure of a periodic system built of alternating left- and right-handed dielectric slabs contains conical singularities similar to the Dirac points in the energy spectrum of charged quasiparticles in graphene. Such singularities in the zone structure of the infinite systems give rise to rather unusual properties of light transport in finite samples. In an insightful numerical experiment (the propagation of a Gaussian beam through a mixed stack of normal and metadielectrics), we simultaneously demonstrate four Dirac point-induced anomalies: (i) diffusionlike decay of the intensity at forbidden frequencies, (ii) focusing and defocussing of the beam, (iii) absence of the transverse shift of the beam, and (iv) a spatial analogue of the Zitterbewegung effect. All of these phenomena take place in media with nonzero average refractive index and can be tuned by changing either the geometrical and electromagnetic parameters of the sample or the frequency and the polarization of light.

I. INTRODUCTION

Highly unusual properties of monolayers of graphite (graphene) and of optical media with negative refractive indices (left-handed metamaterials) had been independently predicted and studied theoretically a long time ago.[1,2] At that time, however, these predictions were perceived as rather intriguing but unrealistic exotica and remained unnoticed for about a half-century, until quite recently (and nearly simultaneously), they were embodied in real materials. This immediately triggered an explosion of interest and activities, in metamaterials and graphene, both in solid state physics and optics. Researchers also realized that the most unusual properties of electron transport in graphene were also peculiar to the propagation of light in dielectric systems with metamaterials. Mathematically, this is because, under some (rather general) conditions, the Maxwell equations for electromagnetic waves in an inhomogeneous dielectric medium can be reduced to the Dirac equations for charge carriers in graphene subjected to an external electric potential.

A. Similarities between Maxwell and Dirac equations

The history of recasting Maxwell equations in alternative, more compact, spinor forms goes back to the beginning of the past century, and is still in progress (for a comprehensive historical overview see Refs. 3 and 4, with recent examples in Refs. 5–8). Therefore it is not surprising that the similarity between Maxwell and Dirac equations has long been noticed (according to Ref. 3, Majorana discussed it already in 1930). In the general case of inhomogeneous media, the close analogy between (i) the quantum-mechanical form of the equations for the Reimann-Silberstain vector fields (linear combinations of the electromagnetic vectors $\vec{D}$ and $\vec{B}$) and (ii) the Dirac equation, written in the chiral representation of the Dirac matrices, was explicitly demonstrated in Ref. 3.

Recently, as graphene became increasingly more popular in solid state physics, the mathematically established similarity of Maxwell and Dirac equations took on a new physical significance. Inspired by the very unusual predictions and discoveries made in graphene, research groups in optics started endeavors to reproduce the unique transport properties of graphene in specifically designed dielectric structures. An additional incentive to these efforts came from the fact that, while the elementary building blocks of graphene are fixed, modern micro and nanotechnologies enable manufacturing periodic dielectric samples with a variety of types and sizes of unit cells. Moreover, the electrodynamic parameters of photonic crystals can, in principle, be controlled by external fields, providing unique opportunities to study condensed matter phenomena in optical ways; for example, by opening a gap between Dirac cones, as well as breaking and restoring space-inversion and time-reversal symmetries.[5] Rather simple electrodynamical analogies furnish physical insights into properties and applications of graphene such as the Klein phenomenon,[9] breaking the valley degeneracy,[10] graphene quantum dots,[11,12] the electronic Goos-Hanchen shift,[13] delocalization in one-dimensional disordered systems,[14] etc. Furthermore, some exotic phenomena predicted and discovered in optical systems (like, for example, the "light wheel" localized mode,[15] or confined cavity modes and ministop bands in broad periodic photonic waveguides[16,17]) could prompt unique possibilities for creating new graphene-based devices. In this regard, particularly promising is the analogy between photonic crystal broad waveguides and zigzag graphene nanoribbons studied in Ref. 18, where it was shown that the photonic mode coupling also arises in nanoribbons at low energies.
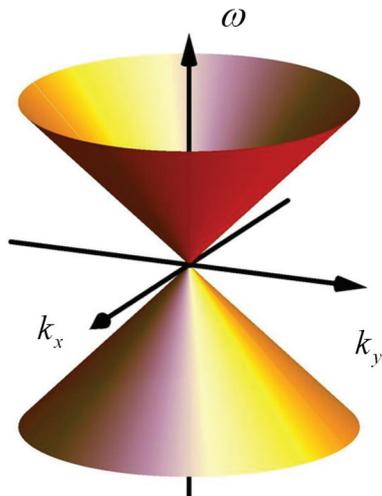
FIG. 1. (Color online) Surface $\omega(k_x, k_y)$ described by the dispersion equation (1) for electromagnetic waves. The contact of two cones looks like a Dirac point in graphene; however, in contrast to graphene, for light, both cones correspond to the same field.

The implementation of the analogy between Dirac electrons and light could be rewarding for the optical community as well, because it is relatively easy to create in graphene an inhomogeneous potential pattern with any distribution of *p-n* and *n-n* junctions, while designing a periodic or random stack of alternating positive-negative dielectric layers is nowadays a feasible task. Thus graphene could provide analogue laboratory models in order to test the optics of metamaterials in a controlled way.

B. Dirac point

The key feature of graphene, from which all its unique transport properties stem, is the existence of Dirac cones in the band structure of its energy spectrum. At first glance, one does not have to work hard to obtain in optics a double-conical, graphenelike dispersion law: it is inherent in any plane monochromatic wave propagating in a homogeneous medium, as the relation between its frequency ω and the wave number k is given by

$$\omega^2 = c^2 k^2. \tag{1}$$

However, the contact of two cones in Fig. 1 only looks like a Dirac point (DP). In fact, of the two cones in Fig. 1, only one (for example, the upper one) is related to a photon, while the second solution of Eq. (1) (lower cone in Fig. 1) is redundant. This lower cone does not carry any additional information and is not related to any different physical entity like, for example, a hole in graphene or a positron in the case of relativistic QED. In other words, the photon and antiphoton are identical.[3] Hence the challenge in optics is to create a structure with a real DP in its spectrum, so that different types of waves would correspond to two different cones (a sort of optical "particle-antiparticle" pair). Appropriate for this purpose are photonic crystals in which two modes degenerated in a homogeneous space become split by the periodicity.[19] The analytical and numerical studies of two-dimensional periodic structures (infinite rods embedded in a background

medium with a different dielectric constant) were carried out as early as in 1991, for square[20] and triangular[21] lattices. Linear singularities (that nowadays are called Dirac points) are clearly seen in the band structures of both systems, although they escaped the attention of Refs. 20 and 21 mostly interested in absolute band gaps for different polarizations. Afterwards, during more than two decades, studies of two-dimensional photonic crystals were primarily aimed on maximizing the photonic band gap[22–24] (see also the review Ref. 25, and references therein), until the discovery of the unusual transport properties in graphene, and the potential to reproduce them in optics switched efforts towards the search and further exploration of photonic structures with Dirac-conelike singularities in their transmission spectra.[5,7,19,26] A number of new optical phenomena arising due to the existence of Dirac points were predicted and discovered: diffusionlike $1/L$-dependence of the pulse intensity on the distance L of propagation inside the photonic crystal[19,27] (which is unusual for nonrandom media), oscillatory motion of a Gaussian beam (optical analogue of the Zitterbewegung effect),[28–30] extinction of coherent backscattering,[31–33] conical diffraction,[34] as well as the existence of graphenelike and novel edge states.[35,36]

From the above-mentioned publications, one can conclude that the existence of Dirac points in *two-dimensional* periodic structures is a rather universal phenomenon, in the sense that they appear irrespective of sample details, such as the shape and dielectric parameters of the "atoms" and its structural symmetry. For example, in the band structures presented in Refs. 7,20,21, and 37, DPs show up at square, triangular, and honeycomb lattices. The general criteria for the existence of DP in periodic dielectric samples were discussed in Ref. 38.

The situation in layered periodic media is quite different and less studied. As we show below, DPs cannot exist in periodically layered dielectric structures built of monotype (i.e., with either all positive or negative refractive indices) dielectrics, no matter their period, size, and dielectric contrast between the layers. In Refs. 38 and 39, a one-dimensional periodic array of metallic unit cells of a special shape was considered, which exhibited Dirac points created by the accidental degeneracy of two modes. To create photonic Dirac cones in one dimension, both normal and metamaterials should be used. Interestingly enough, a single DP can exist in a *homogeneous* dispersive metamedium at a frequency at which both the dielectric permittivity and the magnetic permeability approach zero simultaneously.[6] Eigenwaves in *structured*, infinite periodic systems built of alternating normal and left-handed dielectric layers, and the transmission and reflection from finite samples, were analyzed in Refs. 40–42. It was shown that, when the spatial average of the refractive index over the period was zero, the band structure consisted of gaps at all frequencies except for a set of isolated points (discrete modes), for which the optical thicknesses of the adjacent layers were equal to the same integer number of half-wavelengths. New Dirac cones in graphene supelatices created by double-periodic and quasiperiodic electrostatic potentials have been considered in Ref. 43.

C. Brief summary

Here we study the transport properties of layered periodic dielectric systems "electronically similar" to graphene, in the

sense that they possess Dirac cones in their photonic band gap structures. In Sec. II, we demonstrate, using a simple example, and discuss the similarity and differences between the Maxwell and Dirac equations as well as between the corresponding boundary conditions. Section III presents the transmission through potential barriers created in graphene by applying steplike electrostatic potentials, in comparison with light propagation in slabs of normal dielectrics and metamaterials. In Sec. IV, the photonic band-gap structures of periodically layered dielectrics are compared with the structure of the electron energy zones of graphene subjected to a periodic potential. It is shown that, unlike a two-dimensional photonic crystal, Dirac cones in a layered periodic medium can exist only when the medium consists of alternating slabs of left- and right-handed dielectrics (mixed samples). In Sec. V, we study the propagation of Gaussian beams of light through periodically layered *mixed* samples built of alternating slabs with positive and negative refractive indices, and of beams of charge carriers through finite graphene superlattices. We demonstrate the anomalous, diffusionlike dependence of the intensity on the propagation distance, and an analog of the Zitterbewegung effect in a wide range of parameters. New unusual transport properties of such samples are predicted. In particular, it is shown that two contacting Dirac cones manifest themselves differently: given two beams with frequencies belonging to different cones, one is focused and another is defocused. The magnitude of the shift of the focus is independent on the distance of the sample from the focal plane of the incident beam and is proportional to the width of the sample. At oblique incidence, a Gaussian beam is not displaced along the sample even at nonzero values of the mean value of the dielectric constant.

II. EQUATIONS AND BOUNDARY CONDITIONS

The dynamics of the charge carriers in an external potential u in graphene is described by a spinor

$$\psi = (\psi_A, \psi_B)^T$$

whose components are related to two sublattices in the unit cell of the crystal.[44] In the low-energy limit, near the Dirac point, the components of this spinor obey the Dirac equations. When the energy w of the charge carrier is fixed, then the time dependence of the spinor is given by $\exp(-iwt/\hbar)$, and these equations can be written as

$$
\begin{aligned}
\psi_A &= -\frac{i v_F \hbar}{w - u(x,y)} \left(\frac{\partial \psi_B}{\partial x} - i \frac{\partial \psi_B}{\partial y} \right), \\
\psi_B &= -\frac{i v_F \hbar}{w - u(x,y)} \left(\frac{\partial \psi_A}{\partial x} + i \frac{\partial \psi_A}{\partial y} \right),
\end{aligned}
\tag{2}
$$

where $u(x,y)$ is the electrostatic potential and v_F is the Fermi velocity.

In order to link this to Maxwell equations, we now consider, as an example, a TE electromagnetic wave (where the magnetic field has only one nonzero z component) propagating in a homogeneous medium and introduce two complex-valued functions

$$\mathcal{E} = E_y - iE_x, \quad \mathcal{H} = ZH_z, \tag{3}$$

where $Z = \mu/\varepsilon$ is the medium impedance, μ and ε are the medium permeability and permittivity, accordingly. In Ref. 3, instead of Eq. (3), the Reimann-Silberstain vector wave functions were used to derive a quantum-mechanical matrix form of the classical wave equations in the general case of arbitrary electromagnetic fields propagating in media with space-dependent permittivity and permeability. The analogy with the relativistic Dirac equations was noted.

It is easy to show that for monochromatic fields $\mathcal{E}$ and $\mathcal{H}$ [the time dependence is given by $\exp(-i\omega t)$], the Maxwell equations yield

$$\mathcal{H} = -\frac{i}{k_0 n} \left(\frac{\partial \mathcal{E}}{\partial x} - i \frac{\partial \mathcal{E}}{\partial y} \right), \quad \mathcal{E} = -\frac{i}{k_0 n} \left(\frac{\partial \mathcal{H}}{\partial x} + i \frac{\partial \mathcal{H}}{\partial y} \right). \tag{4}$$

Here, n is the medium refractive index, and $k_0 = \omega/c$. It is evident that after the replacement

$$\mathcal{E} \leftrightarrow \psi_A, \quad \mathcal{H} \leftrightarrow \psi_B, \quad n\omega \leftrightarrow (w-u)/\hbar, \quad c \leftrightarrow v_F, \tag{5}$$

Eq. (4) coincides with Eq. (2). Namely, the 2D Maxwell equations for the complex effective fields (3) in a homogeneous medium and the Dirac equations for the wave functions of the charge carriers in graphene become identical. The role of the refractive index of the corresponding effective medium is played by the quantity $n_{\rm eff} = (w-u)/\hbar\omega$. Therefore, if, for example, the potential is a piecewise-constant function of one coordinate, the corresponding graphene superlattice models a layered dielectric structure.[14] In particular, a layer, in which the potential u exceeds the energy w of the particle, $w - u < 0$, is similar to a slab with negative refractive index n. This means that a junction of two regions having opposite signs of $w - u$ is similar to an interface between left- and right-handed dielectric media with the refractive indices n_1 and n_2, if

$$\frac{n_1}{n_2} = \frac{w - u_1}{w - u_2}. \tag{6}$$

Because of this similarity, a *p-n* junction can focus Dirac electrons in graphene[45] in the same way as the focusing of electromagnetic waves by the boundary between a normal dielectric and a metamaterial.[1,46] However, it is important to realize that, as it follows from Eq. (6), a change of w necessarily implies the corresponding change of the ratio n_1/n_2. Thus, to model the same (i.e., with fixed values of u_1 and u_2) graphene bilayer structure, but at different energies, one has to chose different pairs of dielectrics.

It follows from Eq. (2) that the energy spectrum of the charge carriers in graphene in a homogeneous potential $u = $ const is linear near $k = 0$, i.e., consists of two cones touching at the Dirac point (see Fig. 1):

$$\left(\frac{w - u}{\hbar v_F} \right)^2 = k_x^2 + k_y^2. \tag{7}$$

After substituting Eq. (5), Eq. (7) looks exactly like the dispersion law (1) for photons. Whilst Eqs. (2) and (4) are akin, the similarity between the two problems is not complete. First, unlike Dirac wave functions, the genuine electromagnetic fields $\vec{E}$ and $\vec{H}$ are real, i.e., equal to their complex conjugates. Due to this, positive and negative frequencies (upper and lower cones in Fig. 1) correspond to the same fields, in contrast to

a Dirac spinor, which describes electrons, when $(w - u) > 0$, and holes, when $(w - u) < 0$. One further distinction is that the electric field $\vec{E}$ satisfies the continuity condition

$$\text{div } \vec{E} = \frac{\partial E_x}{\partial x} + \frac{\partial E_y}{\partial y} = 0, \tag{8}$$

which is not required for the Dirac wave functions.

Essentially different are also the boundary conditions for the Dirac wave functions at the interface between two half-spaces with potentials u_1 and u_2,

$$\psi_{1A} = \psi_{2A}, \qquad \psi_{1B} = \psi_{2B}, \tag{9}$$

and for the effective electromagnetic fields $\mathcal{E}$ and $\mathcal{H}$ at the boundary between two dielectrics,

$$Z_2 \mathcal{H}_1 = Z_1 \mathcal{H}_2, \qquad \text{Re } \mathcal{E}_1 = \text{Re } \mathcal{E}_2. \tag{10}$$

Equations (10) follow from the boundary conditions for the real fields, $E_{1y} = E_{2y}$ and $H_{1z} = H_{2z}$ (the boundary is assumed to be parallel to the y axis).

Although the charge transport in graphene and the light propagation in dielectrics are governed by similar equations, Eqs. (2) and (4), inside the medium, the boundary conditions (9) and (10) are distinct from each other. This means that, generally speaking, the coupling between adjacent samples in these two cases is different. This difference is more conspicuous in the particular case of a monochromatic plane wave, $\mathcal{H} \propto \mathcal{E} \propto \exp[i(k_x x + k_y y - \omega t)]$, when the boundary conditions for the effective fields take the form

$$Z_2 \mathcal{H}_1 = Z_1 \mathcal{H}_2, \quad \mathcal{E}(1 + ik_y/k_{2x}) = \mathcal{E}_2(1 + ik_y/k_{1x}), \tag{11}$$

where $k_{jx} = \sqrt{k_0^2 n_j^2 - k_y^2}$. It is easy to see that Eqs. (9) and (11) coincide only when $k_y = 0$ (normal incidence) and $Z_1 = Z_2$. That is, in this particular instance, the transmission of Dirac electrons through a junction is similar to the transmission of light through an interface between two media with different refractive indices but equal impedances. In other words, at normal incidence, any junction in graphene, either *n-n*, *p-p*, or *p-n*, is analogous to a contact between two perfectly matched dielectrics or microwave elements. Such an interface is absolutely transparent to the *normally incident* radiation and therefore to the Dirac electrons in graphene as well. This provides a more intuitive insight into the physics of the Klein paradox (perfect transmission through a high potential barrier[44,47]) in graphene systems.

III. TRANSMISSION THROUGH POTENTIAL BARRIERS AND DIELECTRIC SLABS: SIMILARITIES AND DIFFERENCES

To compare the transport properties of Dirac electrons and light in the general case of oblique incidence, $k_y \neq 0$, we first consider the transmission of particles through a steplike potential barrier, i.e., through the line $x = 0$ separating two domains (1 and 2) of a graphene sheet with different values u_1 and u_2 of the potential. In what follows, we will consider only one spinor component, say $\psi_A \equiv \psi$, because ψ_B could be found using Eq. (2). The solutions of Eq. (2) in both domains can be presented as a linear combination of plane waves with

equal (at the chosen geometry of the system) values of k_y:

$$\psi_j = e^{i[k_y y - (w - u_j)t/\hbar]}[\psi_j^{(+)} e^{ik_{jx}x} + \psi_j^{(-)} e^{-ik_{jx}x}], \quad j = 1, 2. \tag{12}$$

From now on, we consider the range of parameters where there are no total internal reflections and therefore $\text{Im} k_x = 0$. From the continuity of the wave functions at the boundary, Eq. (9), it follows (the incident wave now propagates from medium 1 to medium 2)

$$\begin{pmatrix} \psi_2^{(+)} \\ \psi_2^{(-)} \end{pmatrix} = \hat{M}_{1 \to 2} \begin{pmatrix} \psi_1^{(+)} \\ \psi_1^{(-)} \end{pmatrix}, \tag{13}$$

where the transfer matrix $\hat{M}_{1 \to 2}$ for the interface $x = 0$ is equal to

$$\hat{M}_{1 \to 2} = \frac{1}{2\cos\theta_2} \left\| \begin{matrix} g_{1 \to 2}^{(+)} & g_{1 \to 2}^{(-)} \\ g_{1 \to 2}^{(-)*} & g_{1 \to 2}^{(+)*} \end{matrix} \right\| \tag{14}$$

and the matrix elements are

$$g_{1 \to 2}^{(\pm)} = e^{-i\theta_2} \pm s_1 s_2 e^{\pm i\theta_1}. \tag{15}$$

Here, $s_j = \text{sgn}(w - u_j)$, θ_1 and θ_2 are the angles of incidence and refraction, respectively, while $\theta_j = \arctan(k_y/k_{jx})$.

We determine the transmission T and reflection R coefficients as the ratios of the normal-to-the-boundary components of the densities of the transmitted, $\vec{J}_2^{(+)}$, and reflected, $\vec{J}_1^{(-)}$, currents divided by the normal component of the incident current density $J_{1x}^{(+)}$:

$$T = J_{2x}^{(+)} / J_{1x}^{(+)}, \qquad R = J_{1x}^{(-)} / J_{1x}^{(+)}, \tag{16}$$

where

$$J_{jx}^{(\pm)} = \pm 2 s_j \cos\theta_j |\psi_j^{(\pm)}|^2. \tag{17}$$

From Eqs. (16) and (17), the following formulas can be obtained (see, e.g., Refs. 48 and 49):

$$T = \frac{2\cos\theta_1 \cos\theta_2}{1 + \cos(s_1\theta_1 + s_2\theta_2)}, \qquad R = \frac{1 - \cos(s_1\theta_1 - s_2\theta_2)}{1 + \cos(s_1\theta_1 + s_2\theta_2)}, \tag{18}$$

where the angles of incidence θ_1 and refraction θ_2 are connected by the relation

$$\sin\theta_2 = \frac{w - u_1}{w - u_2} \sin\theta_1. \tag{19}$$

The same signs of s_1 and s_2 correspond to *n-n* (or *p-p*) junctions, while for an *n-p* (or *p-n*) junction $s_1 = -s_2$. It is easy to see that at normal incidence ($\theta_1 = \theta_2 = 0$) the potential barrier of any height is absolutely transparent at any energy (the Klein tunneling effect).

In the case of light propagating through the interface between two dielectrics, whose parameters are ε_1, μ_1 and ε_2, μ_2, the transfer matrix

$$\hat{\mathcal{M}}_{1 \to 2} = \frac{1}{2\cos\theta_2} \left\| \begin{matrix} \mathcal{G}_{1 \to 2}^{(+)} & \mathcal{G}_{1 \to 2}^{(-)} \\ \mathcal{G}_{1 \to 2}^{(-)*} & \mathcal{G}_{1 \to 2}^{(+)*} \end{matrix} \right\| \tag{20}$$

connects the amplitudes of leftward and rightward propagating waves at both sides, and has the same form as Eq. (14), with

the matrix elements $g_{2\to1}^{(\pm)}$ replaced by

$$\mathcal{G}_{1\to2}^{(\pm)} = \cos\theta_2 \pm s_1 s_2 \cos\theta_1 \frac{Z_2}{Z_1} \tag{21}$$

for TE waves and by

$$\mathcal{G}_{1\to2}^{(\pm)} = \cos\theta_2 \frac{Z_2}{Z_1} \pm s_1 s_2 \cos\theta_1 \tag{22}$$

for TM radiation. In Eqs. (21) and (22), $s_j = \operatorname{sgn} n_j$, $n_j = \pm\sqrt{\varepsilon_j \mu_j}$, and $Z_j = \sqrt{\mu_j/\varepsilon_j}$. For left-handed dielectrics ($\varepsilon < 0$, $\mu < 0$), the refractive index n is negative.

When $Z_1 = Z_2$, the expressions (21) and (22) are identical and are related to the matrix elements (15) of the corresponding transfer matrix in graphene, Eq. (13), as

$$\mathcal{G}_{1\to2}^{(\pm)} = \operatorname{Re} g_{1\to2}^{(\pm)}. \tag{23}$$

This relation is a consequence of the above mentioned difference between the solutions of the Dirac and Maxwell equations: the former are complex-valued functions, while the electromagnetic fields are real.

The light transmission and reflection coefficients are determined as the ratios of the normal components of the transmitted (for T) and reflected (for R) energy fluxes divided by the normal component of the incident energy flux. When $Z_1 = Z_2$ (the situation most favorable for the analogy between Dirac electrons and light), T and R take the forms

$$T = \frac{4\cos\theta_1 \cos\theta_2}{(\cos\theta_1 + \cos\theta_2)^2}, \quad R = \frac{(\cos\theta_1 - \cos\theta_2)^2}{(\cos\theta_1 + \cos\theta_2)^2}. \tag{24}$$

One can see that even in the particular case, $Z_1 = Z_2$, Eqs. (18) and (24) are, generally speaking, different, and coincide only when $\theta_1 = \theta_2 = 0$, i.e., when the boundary conditions (11) are equivalent. This means that in spite of the identity of Eqs. (2) and (4), the analogy between the transport of Dirac electrons in graphene and electromagnetic radiation in dielectrics should not be extended too far. Due to the differences in the boundary conditions, the analogy holds only for normal incidence on the interface between two perfectly matched media.

The transmission of Dirac electrons trough a potential barrier of finite width d, and of an electromagnetic wave through a dielectric slab of the same width are described by similar matrices of the form

$$\hat{B} = \hat{A}_{2\to1} \hat{S}_d \hat{A}_{1\to2}, \tag{25}$$

where the indices 1 and 2 now correspond, respectively, to the outside and inside of the barrier (slab). The matrix $\hat{A}$ is equal to $\hat{M}$, as in Eq. (14) for graphene, and $\hat{A} = \hat{\mathcal{M}}$, as in Eq. (20) for dielectrics. Obviously, $\hat{A}_{2\to1}\hat{A}_{1\to2} = \hat{I}$, where $\hat{I}$ is a unit matrix. The diagonal matrix $\hat{S}_d = \operatorname{diag}(e^{i\varphi}, e^{-i\varphi})$, with $\varphi = k_{2x}d$ describes the propagation inside the barrier (dielectric slab). From Eq. (25), it follows that under the condition

$$k_{2x} d = m\pi, \quad m = 1,2,3,\dots, \tag{26}$$

$\hat{B} = (-1)^m \hat{I}$. This means that either a potential barrier or a layer of dielectric is transparent if its width is equal to an integer number of half-wavelengths. This is a general property of both, Dirac and Maxwell equations, which is independent of the ratio between the impedances, and its physical nature has nothing to do with the Klein tunneling.

IV. PERIODICALLY STRIPPED GRAPHENE SUPERLATTICES AND PHOTONIC STRUCTURES

In this section, we compare the structure of the electron energy zones of graphene subject to a periodic electrostatic potential, with the photonic band gap structures of periodically layered dielectrics. To do this, we assume that the potential in graphene takes the two values u_1 and u_2 in alternating areas of widths d_1 and d_2, and the corresponding dielectric sample is built of alternating layers of the same thicknesses, d_1 and d_2, with refractive indices n_1 and n_2, and impedances Z_1 and Z_2, respectively. In both cases, the propagation in the layers 1 and 2 is described by the matrices $\hat{S}_j = \operatorname{diag}(e^{i\varphi_j}, e^{-i\varphi_j})$, $j = 1,2$, where $\varphi_j = d_j k_{jx}$. Assuming that the layers are parallel to the y axis, the transformation matrix $\hat{P}$ on the period $D = d_1 + d_2$ is defined by $\psi(x + D) = \hat{P}\psi(x)$ and is equal to

$$\hat{P} = \hat{S}_1 \hat{M}_{2\to1} \hat{S}_2 \hat{M}_{1\to2} \tag{27}$$

for graphene and

$$\hat{\mathcal{P}} = \hat{S}_1 \hat{\mathcal{M}}_{2\to1} \hat{S}_2 \hat{\mathcal{M}}_{1\to2} \tag{28}$$

for dielectrics.

The eigenvalues $\lambda = \exp(ik_\parallel D)$ ($k_\parallel$ is the Bloch wave number along the x axis) of the matrix $\hat{P}$ ($\hat{\mathcal{P}}$) depend on the energy (frequency) and on the tangent component k_y of the wave vector. Both periodic structures are transparent if

$$|\lambda| = 1. \tag{29}$$

In other words, Eq. (29) determines the transparency zones: the ranges of the energies (frequencies) and wave numbers k_y for which the longitudinal wave number $k_\parallel$ is real.[50] It can be shown that

$$\lambda = F \pm \sqrt{F^2 - 1}, \tag{30}$$

where

$$F(w, k_y) = \cos\varphi_1 \cos\varphi_2 + \left(\tan\theta_1 \tan\theta_2 - \frac{s_1 s_2}{\cos\theta_1 \cos\theta_2}\right)\sin\varphi_1 \sin\varphi_2 \tag{31}$$

for Dirac electrons in graphene and

$$F(\omega, k_y) = \cos\varphi_1 \cos\varphi_2 - \frac{s_1 s_2}{2}\left(\frac{Z_1 \cos\theta_1}{Z_2 \cos\theta_2} + \frac{Z_2 \cos\theta_2}{Z_1 \cos\theta_1}\right)\sin\varphi_1 \sin\varphi_2 \tag{32}$$

for electromagnetic waves in layered dielectrics. In both cases, the eigenmodes obey the dispersion equation

$$\cos(k_\parallel D) = F. \tag{33}$$

It follows from Eqs. (29) and (30) that a periodic structure is transparent for the points in the plane (k_y, w) [or (k_y, ω)] for which the inequality $|F| \leqslant 1$ holds. On the other hand, in each of these two planes, the conditions

$$\varphi_1 = p\pi, \quad p = 1,2,3,\dots,$$
$$\varphi_2 = q\pi, \quad q = 1,2,3,\dots \tag{34}$$

(p and q are positive integer numbers) determine two sets of curves, where $\hat{P}$ and $\hat{\mathcal{P}}$ are equal to $(-1)^{p+q}\hat{I}$. This means that those types of curves belong to transparency zones. It is apparent that since at the crossings of these lines the eigenvalues of the matrices $\hat{P}$ and $\hat{\mathcal{P}}$ are equal to ± 1, such singular crossing points lie at the edges of the zones and represent their points of contact, known as "conical intersection," or "diabolic points" (see, e.g., Ref. 51).

The coordinates, k_{yt} and $k_{0t} = \omega_t/c$, of these points in the plane (k_y, k_0) can be found from Eq. (34):

$$k_{0t}^2 = [(p\pi/d_1)^2 - (q\pi/d_2)^2]/(n_1^2 - n_2^2),$$
$$k_{yt}^2 = [n_2^2(p\pi/d_1)^2 - n_1^2(q\pi/d_2)^2]/(n_1^2 - n_2^2). \quad (35)$$

In the case of graphene, the coordinates of the diabolic points in the plane (w, k_y) are calculated in the same way. In the vicinity of the points defined by Eq. ((34)), the phases φ_1 and φ_2 can be written as

$$\varphi_1 = p\pi + \delta\varphi_1, \qquad \varphi_2 = q\pi + \delta\varphi_2, \quad (36)$$

where $|\delta\varphi_j| \ll 1$. Substituting Eq. (36) into Eq. (32) yields

$$F \simeq (-1)^{p+q}\left[1 - \tfrac{1}{2}\left(\delta\varphi_1^2 + \delta\varphi_2^2 + 2a\delta\varphi_1\delta\varphi_2\right)\right]$$
$$\equiv \left[1 - \tfrac{1}{2}f(\delta\varphi_1, \delta\varphi_2)\right] \quad (37)$$

with

$$a = \frac{s_1 s_2}{2}\left(\frac{Z_1\cos\theta_1}{Z_2\cos\theta_2} + \frac{Z_2\cos\theta_2}{Z_1\cos\theta_1}\right)$$
$$\equiv \frac{1}{2}\left(\frac{k_{1x}\varepsilon_2}{k_{2x}\varepsilon_1} + \frac{k_{2x}\varepsilon_1}{k_{1x}\varepsilon_2}\right),$$

where the components k_{1x} and k_{2x} are taken at the point (k_{yt}, k_{0t}). In the plane $(\delta k_y, \delta k_0)$, where δk_0 and δk_y are small deviations of k_0 and k_y from their values given by Eq. (35), the points for which the quadratic form $f(\delta\varphi_1, \delta\varphi_2)$ (37) is positive, constitute a transparency zone, while the points with $f < 0$ correspond to a gap in the photonic spectrum.

The relation between $\delta\varphi_j$, δk_y, and δk_0 follows from the formula

$$\varphi_j = d_j\sqrt{n_j^2(k_0)k_0^2 - k_y^2}, \quad (38)$$

where $n_j(k_0)$ is the refraction index of the jth layer. An analogue formula for graphene has the form

$$\varphi_j = d_j\sqrt{[(w - u_j)/\hbar v_F]^2 - k_y^2}. \quad (39)$$

While in conventional dielectrics, the dispersion can be ignored, if it is weak enough, in left-handed materials, it must always be taken into account. Indeed, the surface $\omega(k)$, where $k = \sqrt{k_x^2 + k_y^2}$, for normal dielectrics, is a cone similar to the one presented in Fig. 1; i.e., $\omega(k) = n^{-1}ck$, with $n = \text{const} > 0$. For left-handed metamaterials $n < 0$, and the group velocity $v_g = (d\omega/dk)$ is negative, $v_g < 0$, i.e., is antiparallel to the phase velocity ω/k. The surface $\omega(k)$, in a small vicinity of a certain frequency ω_0, has the form depicted in Fig. 2. Although locally it looks like a part of the lower cone in Fig. 1, $\omega(k) \neq n^{-1}ck$, with $n = \text{const}$ on this surface, because the contact point of the cones is shifted from the origin.

Although the absolute values of the transmission and reflection coefficients in Eqs. (18) and (24) are different, the
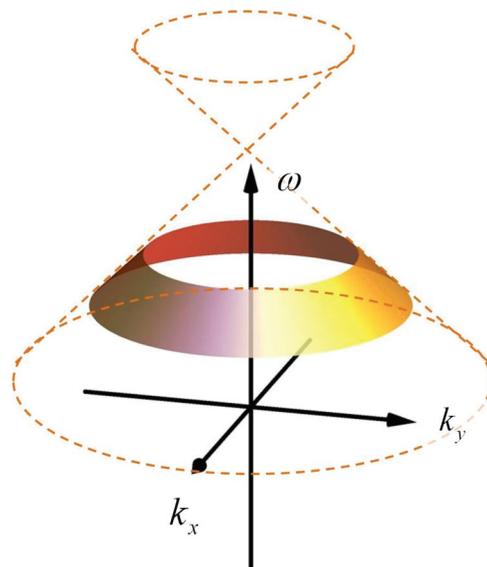

FIG. 2. (Color online) Surface $\omega(k_x, k_y)$ in a small vicinity of a certain frequency for left-handed media.

dispersion characteristics of two adjoining right- and left-handed dielectric layers, and the energetic spectrum diagrams of n-p junction in graphene are identical, as it is shown schematically in Fig. 3. As a consequence of this identity, the periodic dielectric structure and graphene superlattice formed by a periodic external potential possess the same unique transport properties.

A. Photonic structure

From Eq. (38), we obtain

$$\delta\varphi_j = \frac{d_j}{k_{jx}}\left(\frac{ck_{jt}}{v_{jg}}\delta k_0 - k_{yt}\delta k_y\right), \quad (40)$$

where v_{jg} is the wave group velocity in the jth layer at the frequency $\omega_t = ck_{0t}$. The group velocity in Eq. (40) is positive
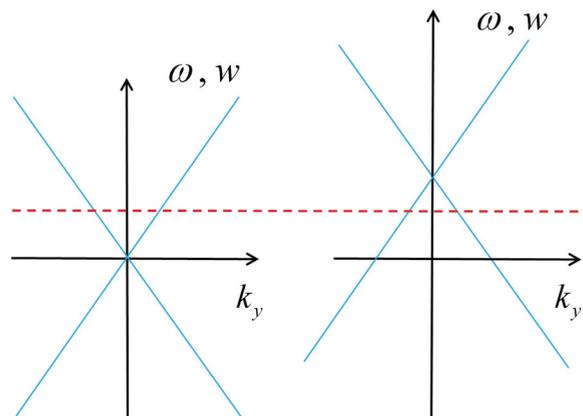

FIG. 3. (Color online) The dispersion characteristics $\omega(k)$, shown as blue lines, of two adjoined right-handed (left panel) and left-handed (right panel) dielectric layers is identical to the energetic spectrum $w(k_y)$ of n-p junction in graphene. The horizontal dashed red line represents the wave frequency, or the quasiparticle energy. The cones' apexes correspond to the zones touching points.

for normal dielectric layers, and negative for layers of left-handed metamaterials.

Equation (40) shows that the phase variations $\delta\varphi_j$ vanish on the lines

$$\delta k_0 = \frac{v_{jg}k_{yt}}{ck_{jt}}\delta k_y. \qquad (41)$$

These lines lie in the transparency zones and intersect at the point where they touch. The line associated with the right-handed dielectric lies in the first and the third quadrants, whereas the line associated with the left-handed metamaterial lies in the second and the fourth quadrants, as it is shown in Fig. 4. When the lattice is composed of conventional dielectrics only, both lines $\delta\varphi_1(\delta k_y,\delta k_0) = 0$ and $\delta\varphi_2(\delta k_y,\delta k_0) = 0$ lie in the first and the third quadrants, and the transparency zones touch one another in a manner shown in Fig. 4(a). There are band gaps above and below the frequency $\omega_t = ck_{0t}$, and these
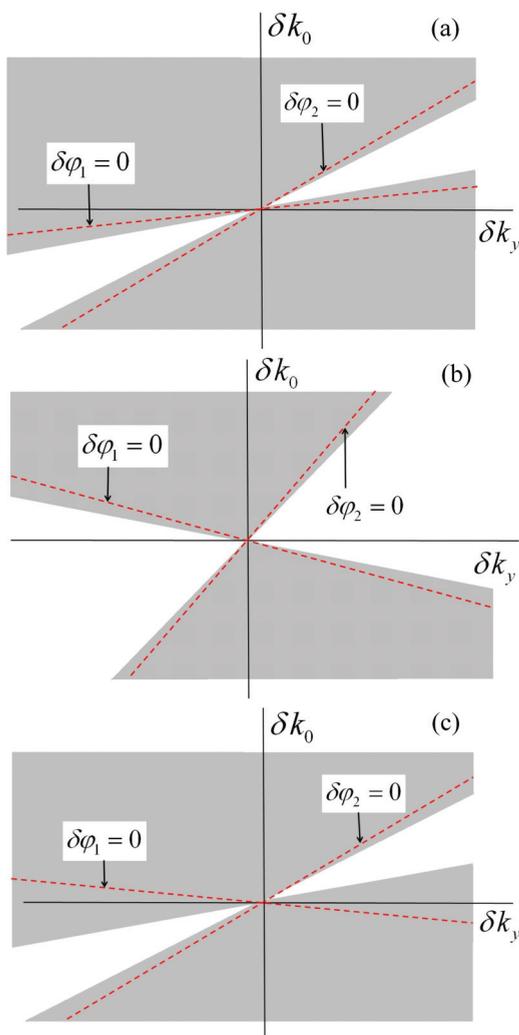
gaps are degenerate in *pointlike nontransparent zones (gaps)* at the frequency $\omega = \omega_t$. Note that the zone structure of the lattice composed of both left-handed dielectrics is similar to the one shown in Fig. 4(a), but symmetrically reflected with respect to the δk_0 axis.

The band structure can be significantly different when the lattice contains both left- and right-handed dielectrics. In this case, there are transparency zones above and below the frequency $\omega_t = ck_{0t}$ that touch one another at the frequency $\omega = \omega_t$, forming a *pointlike transparent zone* as it is shown in Fig. 4(b). This band structure is similar to the energy spectrum of the charge carriers in graphene, and manifests genuine Dirac points. It must be emphasized that for such points to exist, the layers with both positive and negative refractive indices must be present, but the average (over the period) value of n should not necessarily be equal to zero. Materials with effective ε and/or effective μ near zero have become recently the subject of intensive investigation due to their unusual transport properties, including the existence of conical singularities in the band gap structures,[37,52,54–56] however, this topic lies outside the domain of our paper.

It is worth noting that the zone structures shown in Fig. 4 have been calculated for TE (p-polarized) waves. In the case of s-polarized fields, the dielectric permittivities ε_i in Eq. (37) are replaced by the magnetic permeabilities μ_i, therefore the photonic band structure is different, while the coordinates of the diabolic points are the same. This means that for a given frequency and angle of incidence, the same sample could be transparent for s polarization and opaque p polarization, and vice versa. This property can by utilized for the separation of polarizations.

The transparency zones depicted in Fig. 4 are the projections onto the plane (k_y,k_0) of the surface $\omega = \omega(k_x,k_y)$, described by the dispersion equation (33) and shown in Fig. 5. The zone structures, presented in Figs. 4(a), 4(c), and 4(b), correspond to the surfaces shown in Figs. 5(a) and 5(b), respectively.

It is important to note that the presence of both left- and right-handed dielectrics in the periodic structure is a *necessary, but not sufficient* condition for the graphenelike band structure to exist. Generally speaking, the lines (41) and the band edges do not coincide, and can be widely separated. When the distance between the lines (41) and the zone edges is large enough, as, for example, in Fig. 4(c), the zones shape is similar
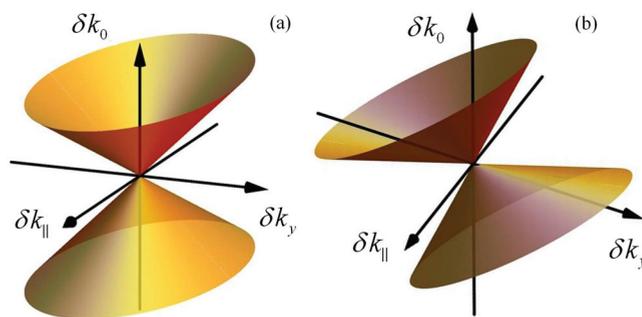

FIG. 4. (Color online) Transparency zones (gray) in the plane $\omega(k_x,k_y)$ for (a) a lattice composed of conventional dielectrics only; (b) and (c) lattices containing both left- and right-handed dielectrics. In (b), the touching point between the zones provides a pointlike transparent zone. In (c), the contact of two zones is a pointlike nontransparent gap. The phase deviations $\delta\varphi_{1,2}$ vanish on the red dashed lines.

FIG. 5. (Color online) Surfaces $\delta k_0(\delta k_\|,\delta k_y)$ for (a) the zone structure depicted in Fig. 4(b) and (b) the zone structures shown in Figs. 4(a) and 4(c).

to that of a lattice formed by right-handed dielectrics only [see Fig. 4(c)]. A detailed analysis of the zones shape is presented in Appendix.

The fundamental qualitative difference between the zone shapes of mono- and mix-lattices owes its origin to the strong dispersion, which is an inherent characteristic of left-haded media. Ignoring this fact ("for simplicity," as this is sometimes done) leads to wrong results for the zones structure in the vicinity of their contact.

Indeed, assuming a constant refractive index $n_j(k_0) =$ const, the phase variation $\delta\varphi_j$ can be written as

$$\delta\varphi_j = \frac{d_j}{k_{jx}} \left(n_j^2 k_0 \delta k_0 - k_y \delta k_y \right), \qquad (42)$$

i.e., the phase variation vanishes on the line that lies in the first and the third quadrants, independently of the sign of n_j.

B. Graphene superlattice

It follows from Eq. (39) that in a graphene superlattice created by an electrostatic potential with periodically alternating values u_1 and u_2, the phase variations $\delta\varphi$ vanish on the lines

$$\delta w = \frac{\hbar^2 v_F^2 k_{yt}}{w_t - u_j} \delta k_y, \qquad (43)$$

where w_t and k_{yt} are the coordinates of the zone touching point in the plane (k_y, w). The slopes of these lines have opposite signs when the energy w_t lies between the values u_1 and u_2 of the potential, i.e., when $\text{sgn}[(w - u_1)(w - u_2)] = -1$. In this case, the zones touch each other either as it is shown in Figs. 4(b) or 4(c) (depending on the relation between the layer thicknesses d_1 and d_2, and the touching point indices p and q). In the opposite case, when $\text{sgn}[(w - u_1)(w - u_2)] = +1$, the zone structure is similar to the one shown in Fig. 4(a), or symmetrically reflected with respect to the ordinate axis. Thus the pointlike transparent zones (new Dirac points) can appear in the graphene superlattice only in the energy range between u_1 and u_2.

V. TRANSMISSION NEAR THE DIRAC POINTS

As it was mentioned in Introduction, the similarity between the energy spectra of electromagnetic waves in homogeneous media and Dirac quasiparticles is only formal and physically meaningless, because the two cones in the photon spectra are identical. To demonstrate that the singular points (presented above) in the band gap structure of mixed periodic dielectric samples possess the properties that make them *bona fide* Dirac points, we considered the transmission of a monochromatic wave of a frequency ω through a finite stack of alternating left- and right-handed dielectric slabs. The dependencies of the amplitudes and phases on the complex transmission coefficients $t(k_y)$ of the y component of the wave vector [i.e., of the angle of incidence $\theta = \arcsin(ck_y/\omega)$] are shown in Figs. 6(a) and 6(b), for two different frequencies belonging, respectively, to the upper and the lower cones in Fig. 2. While the amplitudes $|t(k_y)|$ are similar, the phases $\beta = \arg t(k_y)$ manifest quite distinct behaviors:

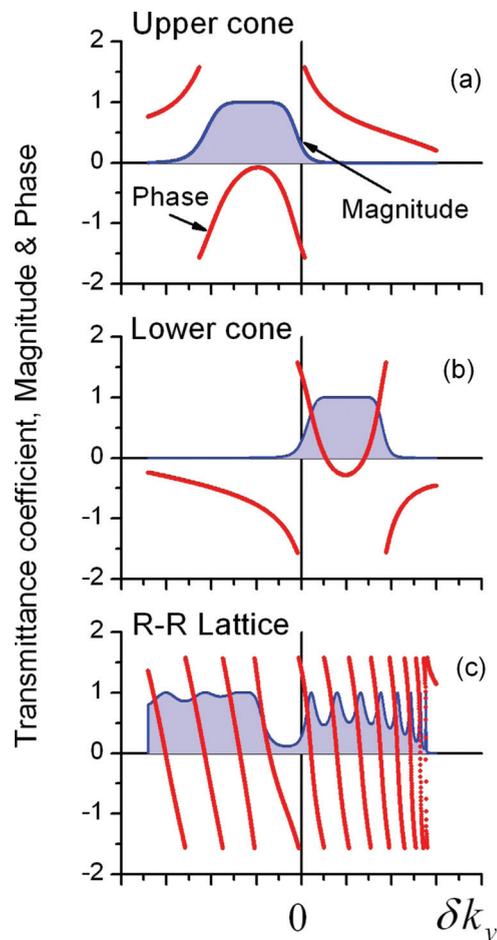$$\beta(k_y) \simeq \pm b(k_y - k_{ym})^2, \qquad (44)$$

FIG. 6. (Color online) The magnitude (blue) and the phase (red) of the complex transmission coefficient $t(k_y)$ of a monochromatic wave propagating through [(a) and (b)] finite periodic stacks of alternating left- and right-handed dielectric layers and (c) a stack of normal dielectric layers. The frequencies in (a) and (b) belong to the upper and lower cones in Fig. 2, respectively. The k_y component of the wave vector determines the angle of incidence $\theta = \arcsin(ck_y/\omega)$. The parameters of the numerical simulations used here are number of periods $N = 9$, $p = 1$, $q = 8$, $d_1 = 0.35D$, $\varepsilon_1 = n_1 = 1$, $|\varepsilon_2| = 0.8$, $|n_2| = 2.5$, $|v_{2g}| = 0.25c$, and $D|\delta k_0| = 0.05$.

where opposite signs correspond to two different cones, and k_{ym} is the position of the phase $\beta(k_y)$ extremum. For comparison, the dependencies of $|t(k_y)|$ and $\beta(k_y)$ for a periodic stack of normal dielectric layers are shown in Fig. 6(c). In this case, the phase is a monotonic (close to linear) function of the angle of incidence at all frequencies and has no singularities at $k_y = k_{yt}$.

Exactly the same parabolic dependence of the phase $\beta(k_y)$ of the transmission coefficient is intrinsic to graphene superlattices, when the contact point corresponds to the pointlike transparent zone. The dependencies of the amplitudes and phases of the complex transmission coefficients $t(k_y)$ on the y component of the wave vector are shown in Fig. 7 for two different energies: one above [see Fig. 7(a)] and another below [see Fig. 7(b)] the energy w_t of the zones contact.
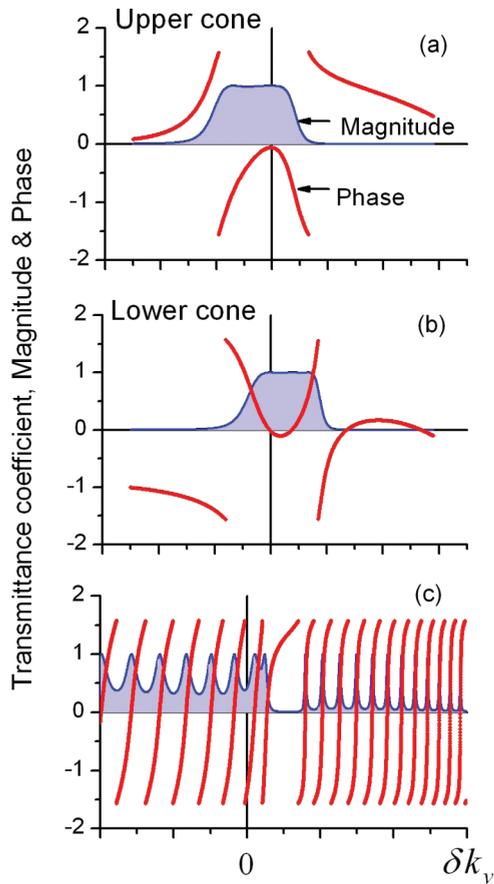
FIG. 7. (Color online) Magnitude (blue) and phase (red) of the complex transmission coefficient $t(k_y)$ of a monoenergetic quasiparticle propagating through [(a) and (b)] a finite periodic set of alternating p-n and n-p junctions in graphene. The quasiparticle energies are (a) above and (b) below the energy of the zones touching w_t. The indexes of the zones contact point are $p = 1$, $q = 5$, and the layer thicknesses are $d_1 = 0.3D$ and $d_2 = 0.7D$. In the same lattice, the zones contact point, whose indexes are $p = 3$ and $q = 1$, corresponds to a pointlike gap, and the dependence $t(k_y)$ looks like the one for a periodic stack of normal dielectrics [see Fig. 6(c)].

As it was mentioned above, the presence of both left- and right-handed dielectrics, or alternating p-n and n-p junctions in graphene, is not sufficient for a point of zone touching to be a pointlike transparency zone (Dirac point). In the same lattice, points of the zone- touching with different indexes p and q can be either pointlike gaps, as shown in Fig. 7(c), or pointlike transparent zones, i.e., Dirac points [see Figs. 7(a) and 7(b)].

A number of interesting effects emerge in the vicinity of the Dirac point of the mixed periodic sample or graphene superlattice. Some of them are caused by the parabolic dependence (44) of the transmittance coefficient phase on the angle of incidence (of k_y). Let us consider the propagation of a monochromatic beam of light, bounded in the transverse dimension (Gaussian beam, for instance), through the mixed stack of a thickness L. Generally, a beam transmitted through a slab of a normal dielectric is shifted along the surface, as it is schematically shown in Fig. 8(a).
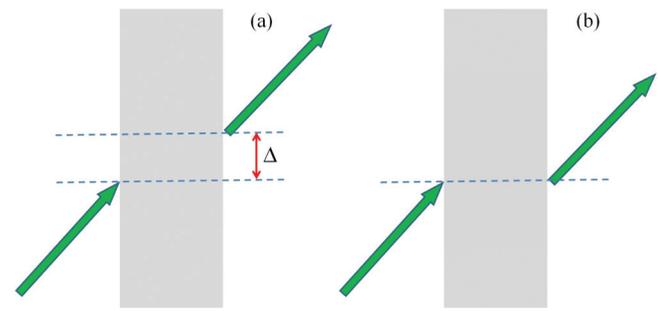

FIG. 8. (Color online) (a) A beam of light transmitted through a slab of a normal dielectric is shifted along the surface. The shift of the beam passing through a mixed periodic stack is much smaller, can be either positive or negative, or even equal to zero, as shown in (b).

The shift Δ is determined[53] by evolution of the phase β of the transmission coefficient t:

$$\Delta = -\left.\frac{d\beta(k_y)}{dk_y}\right|_{k_y=k_{y0}},\qquad(45)$$

where k_{y0} is the tangential component of the wave vector of the central ray in the incident beam. It is assumed in Eq. (45) that the angular width Δk_y of the incident beam is rather small. Since mixed periodic stacks are characterized by the parabolic dependence $\beta(k_y)$, Eq. (44), $d\beta(k_y)/dk_y$ is small or even equal to zero, in which case the longitudinal shift Δ is absent completely.

The absence of the longitudinal shift, when $d\beta(k_y)/dk_y|_{k_y=k_{y0}} = 0$, can also be observed in the so-called near-zero-index metamaterials[57] and in 1D periodic lattices with birefringent materials.[58] It is important to note that in our case, this phenomenon has a different physical origin.

The parabolic dependence $\beta(k_y)$ affects also the curvature of the transmitted beam phase front, i.e., it shifts the focal plane of the incident Gaussian beam. The value Δ_f of this shift is proportional to the thickness L of the mixed stack and is independent of the stack position on the beam trajectory. The sign of the shift Δ_f depends on the sign of the detuning of the beam frequency ω from the Dirac-point frequency ω_t. The focal plane is shifted forward (defocusing) when $\omega < \omega_t$, and backward (focusing) when $\omega > \omega_t$.

This surprising focusing properties of mixed periodic samples are demonstrated in Fig. 9. Of the two beams with the frequencies resting on two different dispersive cones, the one corresponding to the upper cone is focused by the sample, blue curve, while the other (lower cone) is defocused, red line. For comparison, the black curve presents the intensity distribution in the beam propagated in free space. This phenomenon is highly unusual by itself and also reinforces the similarity of the contact points of the cones to a genuine "optical" Dirac point: different cones are not identical, and represent objects with distinct physical properties—a sort of optical particle-antiparticle pair.

When the frequency ω of the incident beam coincides with a pointlike gap of the corresponding infinite structure, i.e., $\omega = \omega_t$, one would expect an exponential decay of the transmitted beam intensity I_{tr} as a function of the mixed stack thickness L: $I_{\text{tr}}(L) \propto \exp(-\gamma L)$. However, the well-pronounced constant
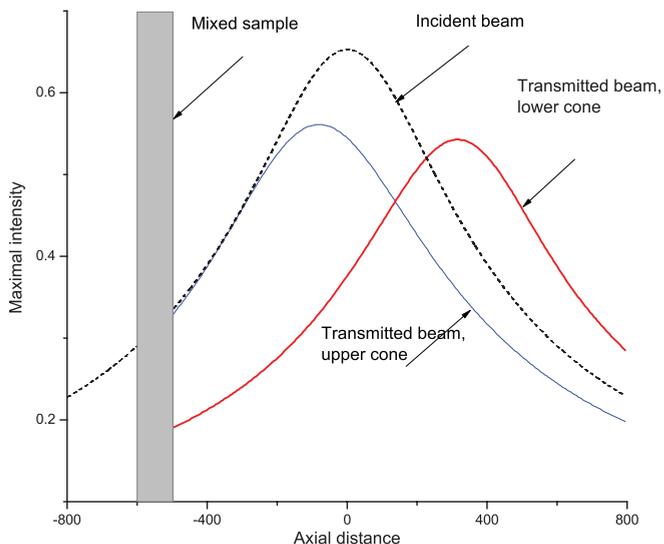
FIG. 9. (Color online) Focusing properties of a mixed periodic sample. After the transmission through a mixed periodic sample (grey area), the focus of the beam with a frequency belonging to the upper cone (blue curve) is shifted to the left with respect to the beam propagating in free space (black curve). The same sample shifts the focus of the beam with frequency from the lower cone (red curve) in the opposite direction. The parameters of the numerical simulations used here are the number of periods $N = 100$, $p = 2$, $q = 5$, $d_1 = 0.4D$, $\varepsilon_1 = n_1 = 1$, $\varepsilon_2 = -0.5$, $n_2 = -0.5$, $v_{2g} = -0.6c$, and $D|\delta k_0| = 0.3$.

asymptotic of the function $L\, I_{tr}(L)$ (see Fig. 10, red line), demonstrates an anomalously high intensity, decaying as $1/L$. Such a diffusionlike dependence is one of the consequences of the linear, Dirac conelike dispersion. In two-dimensional photonic crystals with triangular lattices of normal dielectric rods, this phenomenon was predicted in Ref. 19. In layered structures, it could take place only in the presence of left-handed elements.

Because of the similarity between the energy spectrum of relativistic electrons and the frequency band structure of a mixed periodic dielectric structure, it is natural to assume that the light beam propagation into 1mixed samples can be accompanied by a Zitterbewegunglike phenomenon. Indeed, the spatial distribution of the energy flux inside the mixed sample manifests a *trembling motion*: the "center of gravity" of the flux oscillates in the transverse direction (along the y axis). In Fig. 11, the spatial distribution of the energy flux inside the mixed sample is shown. The oscillatory motion of the center of gravity $I_c(y)$ is clearly seen in Fig. 12. Note that Fig. 11 is similar to Fig. 3 in Ref. 59, where the probability function of a moving electron (solution of the Dirac equation) is shown.

Figure 11 also demonstrates the two above-mentioned effects: the absence of the longitudinal shift (the energy propagates normally to the sample boundary, whereas the angle of incidence of the beam is far from the normal) and the focusing of the beam.

All these effects—the absence of the longitudinal shift, the focusing of the beam, and the Zitterbewegung phenomenon—are also seen in graphene superlattices. As an example, the current density distribution in the Gaussian beam of
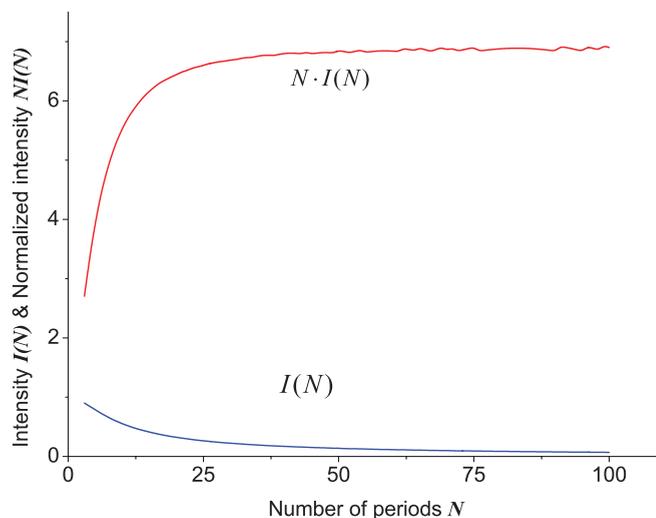

FIG. 10. (Color online) Intensity $I(N)$ (blue line) of the transmitted beam as a function of the distance of propagation inside a mixed stack. The distance is measured in the numbers of periods N. The frequency ω of the incident beam belongs to a pointlike transparency zone (Dirac point) of the corresponding infinite structure, $\omega = \omega_t$. The large-N asymptotic of the red line, $N I(N)$, is constant, which means that the intensity is inversely proportional to the distance (diffusionlike dependence). The parameters of the numerical simulations here are $p = 1$, $q = 8$, $d_1 = 0.35D$, $\varepsilon_1 = n_1 = 1$, $\varepsilon_2 = -0.8$, $n_2 = -2.5$, and $v_{2g} = -0.25c$.

monoenergetic charge carriers propagating through a finite graphene superlattice is depicted in Fig. 13.

Let us now compare the wave propagation through a mixed dielectric slab or a graphene superlattice with the transmission of an electromagnetic wave through a plate made of a *homogeneous* (right- or left-handed) dielectric.
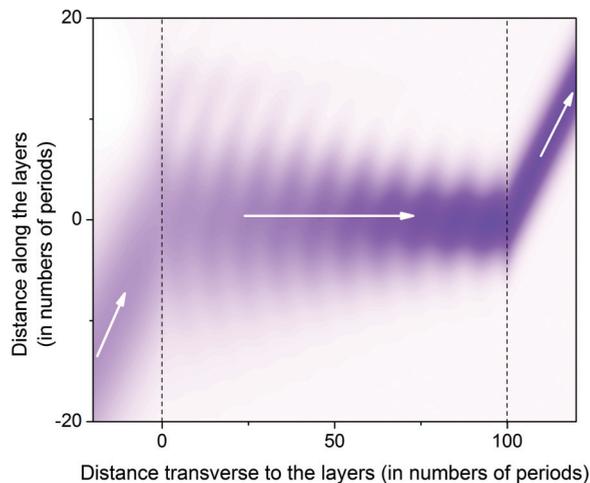

FIG. 11. (Color online) Spatial distribution of the energy flux of the beam propagating (from left to right) through the mixed sample. The angle of incidence $\simeq 34°$. The boundaries of the sample are marked by the vertical dashed lines. The "center of gravity" of the flux oscillates in the transverse (along the y axis) direction. The parameters of the numerical simulations used here are the number of periods $N = 100$, $p = 4$, $q = 10$, $d_1 = 0.4D$, $\varepsilon_1 = n_1 = 1$, $\varepsilon_2 = -0.5$, $n_2 = -1.5$, $v_{2g} = -0.2c$, $D\delta k_0 = -0.07$, and $D\delta k_y = 0.5$.
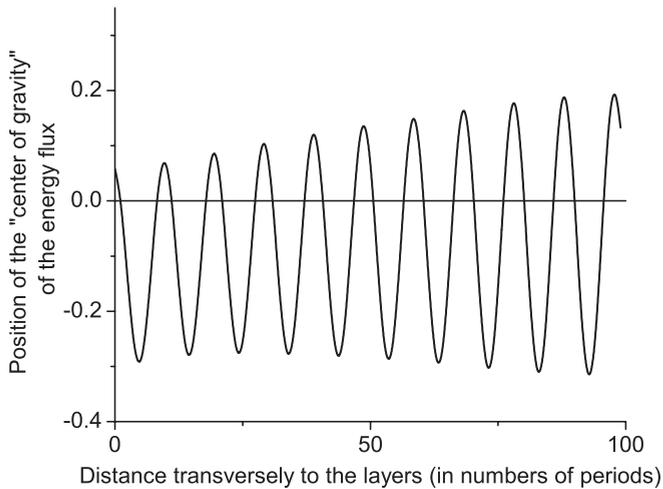
FIG. 12. Oscillations of the transverse coordinate of the "center of gravity" of the beam propagating in the mixed sample.

In a small vicinity of the normal angle of incidence, the dependence $\beta(k_y)$ of the transmission coefficient phase β on the tangential component of the wave number k_y (the dependence on the angle of incidence) has the same parabolic form as discussed above [see Eq. (44)], with the only difference that at homogeneous dielectric plates, $k_{yt} = 0$ by definition:

$$\beta(k_y) = \pm b k_y^2. \tag{46}$$

Here, the plus sign corresponds to right-handed dielectrics, while the minus sign corresponds to left-handed dielectrics. In the first case, the refraction is positive, i.e., the incident beam and the beam inside the plate lie on opposite sides from the normal, whereas in the second case, the beams lie on the same side of the normal (negative refraction). Therefore the
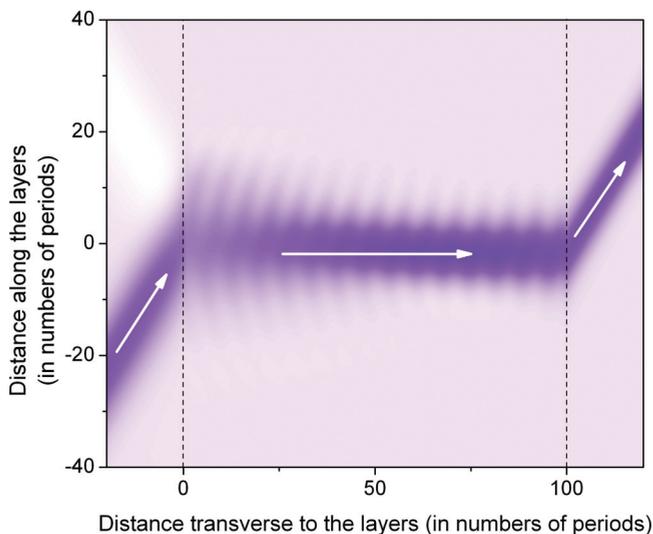

FIG. 13. (Color online) Transmission of the Gaussian beam of charge carriers through a periodic set of *p-n* and *n-p* junctions in graphene near a pointlike gap. The angle of incidence $\simeq 48°$. The sample boundaries are marked by the vertical dashed lines. The parameters of the numerical simulations used here are the number of periods $N = 100$, $p = 1$, $q = 5$, $d_1 = 0.3D$, $u_1 = -u_2 = 20\hbar v_F/D$, $\delta w = -0.3\hbar v_F/D$, and $D\delta k_y = 0.2$.

shift Δ is positive for plates of a right-handed dielectric, and negative for left-handed dielectrics. In other words, in normal samples, k_y and Δ have the same signs, while in metamaterials the signs are opposite. Amazingly, these two situations, each inherent to *different* kinds of homogeneous materials, can be observed in the *same* mixed periodically layered sample, and graphene superlattice. Indeed, depending on which side of the Dirac point the frequency lies, the refraction is either positive (upper cone) or negative (lower cone). In this regard, it is more appropriate to refer to these two cones as a "medium-antimedium" pair, rather than "particle-antiparticle," as in homogeneous graphene.

VI. CONCLUSIONS

We have shown that some of the exotic properties of charge transport in graphene can be reproduced in the propagation of light through layered dielectric samples. Similarities and distinctions between Maxwell and Dirac equations, and between the corresponding boundary conditions have been studied. Although the equations for the real electric and magnetic fields are essentially different from those for the Dirac electrons, under some conditions they can be reduced to similar form. For example, Eq. (4) for the complex combinations given by Eq. (3) coincides with the Dirac equations (2). Therewith, the role of the refractive index in graphene is played by the difference between properly normalized values of the Fermi energy and the external electrostatic potential [see Eq. (5)]. The boundary conditions for a Dirac quasiparticle incident on a plane separating two areas with different potentials, and for an electromagnetic wave propagating through an interface between two layers of homogeneous dielectrics are, generally speaking, different. They coincide only when the impedances of the layers are equal, and the direction of the propagation is normal to the boundary. It means that at normal incidence, any junction in graphene is analogous to a contact between two perfectly matched dielectrics and therefore is absolutely transparent to normally incident Dirac electrons. This provides a more intuitive insight into the physics of the Klein paradox in graphene.

The analytical and numerical analysis of the photonic band gap structures of infinite periodically layered systems reveals an infinite number of the so-called "diabolic points" (singular points of contact of two transparency zones) in the (ω,θ) spectral diagrams (examples are shown in Fig. 4). A distinction needs to be drawn between two types of these singularities: pointlike transparency zones, like in Figs. 4(a) and 4(c), and pointlike gaps in the spectrum, similar to the one presented in Fig. 4(c). Although all three pictures in Fig. 4 are topologically equivalent, the transport properties of the corresponding *finite* periodic stacks of layers differ drastically in the vicinities of these points. Waves with frequencies lying on opposite sides of the singularities of the first type propagate through the samples in similar ways. In the same time, when two touching spectral cones form a pointlike gap, the electromagnetic radiation interacts with the same sample differently, depending to which cone its frequency belongs. Studies of the propagation of beams of light show that only the diabolic points of this type posses the properties of genuine Dirac points. We demonstrate that in monotype layered structures (i.e., in those built of either

normal or left-handed dielectrics), just the diabolic point of the first type can exist, and conical, Dirac-type singularities appear only in mixed (with alternating left- and right-handed layers) samples. This is in contrast to two-dimensional media where Dirac points were discovered in various types of photonic crystals with normal dielectric elements. It is important to note that the physical nature of the Dirac points that we consider is different from that in systems with zero average value of the refractive index: in mixed layered structures, they are due to the specific strong dispersion (phase and group velocities have different signs) inherent in the elements with negative refraction.

Although the angular dependencies of the transmission and reflection coefficients from a single interface in layered dielectrics and graphene superlatices are different [compare formulas Eqs. (18) and (24)], the spectral properties of these two structures are conceptually identical and entail similar features in the light and charge transport. Considering, as examples, the transmission of the Gaussian monochromatic beams of light and monoenergetic Dirac electrons through the corresponding (dielectric or graphene) samples we predict the following Dirac-point-induced effects: (i) two touching Dirac cones influence the propagation of a beam in different ways: the beam is focused when the frequency (energy) belongs to the upper cone, and is defocused at frequencies (energies) lying in the lower one, (ii) the transverse shift of the beam is anomalously small or even zero, (iii) the decay of the intensity at forbidden frequencies is diffusionlike, and (iv) a spatial analog of the Zitterbewegung effect (i.e., trembling motion of the "center of gravity" of the energy flux) is observed in periodically layered dielectric structures with nonzero average refractive indices and in graphene superlattices.

APPENDIX: BOUNDARIES OF THE TRANSPARENCY ZONES OF PHOTONIC STRUCTURES

Boundaries of the transparency zones in the plane $(\delta k_y, \delta k_0)$ in the vicinity of the zones touching point are defined by the equation

$$\delta\varphi_1^2 + \delta\varphi_2^2 + 2a\delta\varphi_1\delta\varphi_2 = 0, \qquad (A1)$$

where $\delta\varphi_j$ are defined by Eq. (40). It follows from Eq. (A1), that

$$\delta\varphi_2 = (-a \pm \sqrt{a^2 - 1}), \qquad (A2)$$

where

$$a = \frac{1}{2}\left(\frac{k_{1x}\varepsilon_2}{k_{2x}\varepsilon_1} + \frac{k_{2x}\varepsilon_1}{k_{1x}\varepsilon_2}\right).$$

This equation, using Eq. (40), can be presented in the form

$$\delta k_0^{(\pm)} = \delta k_y \frac{k_{yt}}{k_{0t}} \frac{d_2 k_{1x} - d_1 k_{2x}(-a \pm \sqrt{a^2 - 1})}{d_2 k_{1x}\frac{c}{v_{g2}} - d_1 k_{2x}\frac{c}{v_{g1}}(-a \pm \sqrt{a^2 - 1})}. \qquad (A3)$$

When the photonic structure is formed by either right- or left-handed layers only, i.e, $a > 0$ and $\mathrm{sgn}(v_{g1}/v_{g2}) = 1$, both lines $\delta k_0^{(\pm)}(\delta k_y)$ lie in the same quadrants and the zones touching point forms a pointlike gap, as it is shown, for instance, in Fig. 4(a). In the mixed structure, which contains both left- and right-handed layers, i.e., $a < 0$ and $\mathrm{sgn}(v_{g1}/v_{g2}) = -1$, the situation is quite different. The denominator in Eq. (A3) has the same sign for both $\delta k_0^{(+)}$ and $\delta k_0^{(-)}$, while the signs of the numerator *can* be different. Whether the sign of $(\delta k_0^{(+)}/\delta k_0^{(-)})$ is equal to -1 or $+1$ depends on the values of the parameters. The zones structures in the first [$\mathrm{sgn}(\delta k_0^{(+)}/\delta k_0^{(-)}) = -1$] and the second [$\mathrm{sgn}(\delta k_0^{(+)}/\delta k_0^{(-)}) = +1$] cases are similar to ones shown in Figs. 4(b) and 4(c), respectively.

Thus the zones touching point presents the pointlike transparent zone when the following inequalities hold:

$$\frac{d_2 k_{1x}}{d_1 k_{2x}} < |a| + \sqrt{a^2 - 1}, \quad \frac{d_2 k_{1x}}{d_1 k_{2x}} > |a| - \sqrt{a^2 - 1}. \quad (A4)$$

Using the definition of the parameter a and Eq. (35) these inequalities can be written as

$$\left(\frac{d_1}{d_2}\right)^3 \left(\frac{q}{p}\right)^2 \left(\frac{\varepsilon_1}{|\varepsilon_2|}\right) < 1 < \left(\frac{d_1}{d_2}\right)\left(\frac{|\varepsilon_2|}{\varepsilon_1}\right), \quad (A5)$$

when

$$\left(\frac{d_2}{d_1}\right)\left(\frac{p}{q}\right)\left(\frac{|\varepsilon_2|}{\varepsilon_1}\right) > 1,$$

and reverse to Eq. (A5) inequalities, when

$$\left(\frac{d_2}{d_1}\right)\left(\frac{p}{q}\right)\left(\frac{|\varepsilon_2|}{\varepsilon_1}\right) < 1.$$

As it follows from Eq. (35), the range of allowed values of the parameters is restricted by the condition

$$\left(\frac{d_2}{d_1}\right)\left(\frac{p}{q}\right)\left(\frac{|n_2|}{n_1}\right) > 1, \qquad (A6)$$

when $n_1 > |n_2|$, and by the reverse inequality when $n_1 < |n_2|$. All these inequalities select a region in the 4-dimensional space of parameters d_1/d_2, p/q, $\varepsilon_1/|\varepsilon_2|$, and $n_1/|n_2|$, where the vicinity of the zones contact point is characterized by the Diraclike spectrum.

Any metamaterial-dielectric pair is characterized by its own values of the parameters $\varepsilon_1/|\varepsilon_2|$ and $n_1/|n_2|$. Therefore, considering these parameters as given, one can define the corresponding area in the two-dimensional space of parameters

$\xi = p/q$ and $\eta = d_1/d_2$ (remainder: p and q are integer numbers). Introducing the notations $A = n_1/|n_2|$ and $B = \varepsilon_1/|\varepsilon_2|$ we can write the inequalities Eqs. (A5) and (A6) as

$$B\eta^3 < \xi^2, \quad \eta < B, \quad B\eta < \xi,$$
$$B\eta^3 > \xi^2, \quad \eta > B, \quad B\eta > \xi, \tag{A7}$$

and

$$\xi > A\eta, \quad \text{if} \quad A > 1,$$
$$\xi < A\eta, \quad \text{if} \quad A < 1. \tag{A8}$$

Equation (A8) means that the line $\eta = A^{-1}\xi$ divides the plane (ξ, η) in two parts. The allowed values of variables ξ and η lie below this line if $A > 1$, and above the line if $A < 1$. Inequalities Eq. (A7) bound an area between the line $\eta = B$ and the curve $\eta = (x^2/B)^{1/3}$. The region where a touching point of the zones presents the genuine Dirac point is defined by the intersection of these two areas, as it is shown in Fig. 14.

Note that the group velocities v_{g1} and $|v_{g2}|$ are not involved in this analysis. These velocities define the angle of opening of the Dirac spectrum, but not the fact of its existence.

Usually, metamaterials exhibit their left-handed properties in a rather narrow frequency range. Because the above-mentioned region is defined only by the relation between the layer thicknesses d_1 and d_2, one can tune the Dirac point
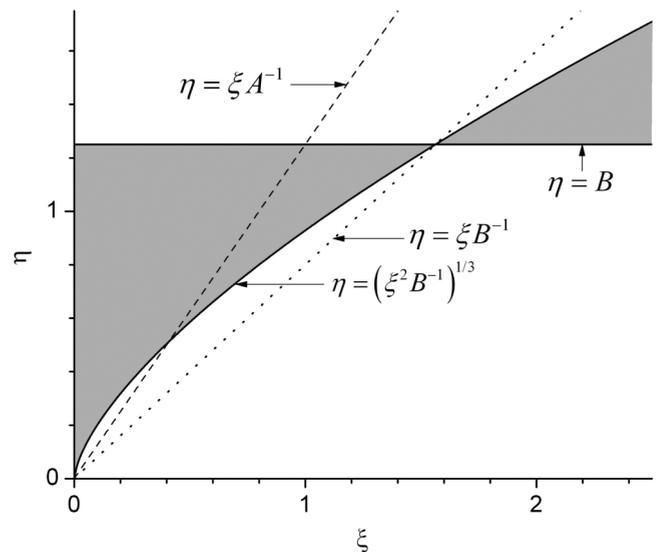

FIG. 14. Plot of the photonic structure parameters $\xi = d_1/d_2$ and $\eta = p/q$. The vicinity of the zones contact point is characterized by a Diraclike spectrum when the structure parameters belong in the gray region below the dashed line (if $A = n_1/|n_2| > 1$) or above this line (if $A = n_1/|n_2| < 1$).

frequency $\omega_t = ck_{0t}$ by an appropriate choice of the structure period D.

[1] V. G. Veselago, Sov. Phys. Usp. **10**, 509 (1968).

[2] P. R. Wallace, Phys. Rev. B **71**, 622 (1947).

[3] I. Bialynicki-Birula, Progress in Optics **36**, 245 (1996).

[4] I. Bialynicki-Birula and Z. Bialynicka-Birula, J. Phys. A: Math. Theor. **46**, 053001 (2013).

[5] F. D. M. Haldane and S. Raghu, Phys. Rev. Lett. **100**, 013904 (2008).

[6] L.-G. Wang, Z.-G. Wang, J.-X. Zhang, and S.-Y. Zhu, Opt. Lett. **34**, 1510 (2009).

[7] T. Ochiai and M. Onoda, Phys. Rev. B **80**, 155103 (2009).

[8] K. Y. Bliokh, A. Y. Bekshaev, and F. Nori, New J. Phys. **15**, 033026 (2013).

[9] A. V. Shytov, M. S. Rudner, and L. S. Levitov, Phys. Rev. Lett. **101**, 156804 (2008).

[10] J. L. Garcia-Pomar, A. Cortijo, and M. Nieto-Vesperinas, Phys. Rev. Lett. **100**, 236801 (2008).

[11] P. Darancet, V. Olevano, and D. Mayou, Phys. Rev. Lett. **102**, 136803 (2009).

[12] A. V. Rozhkov, G. Giavaras, Y. P. Bliokh, V. Freilikher, and F. Nori, Phys. Rep. **503**, 77 (2011).

[13] X. Chen, P.-L. Zhao, and X.-J. Lu, arXiv:1111.1753; X. Chen, X.-J. Lu, Y. Ban, and C.-F. Li, J. Optics **15**, 033001 (2013).

[14] Y. P. Bliokh, V. Freilikher, S. Savel'ev, and F. Nori, Phys. Rev. B **79**, 075123 (2009).

[15] R. Polles, A. Moreau, and G. Granet, Opt. Let. **35**, 3237 (2010).

[16] H. Benisty, N. Piskunov, P. K. Kashkarov, and O. Khayam, Phys. Rev. A **84**, 063825 (2011).

[17] H. Benisty and O. Khayam, IEEE J. Quantum Electron. **47**, 204 (2011).

[18] H. Benisty, Phys. Rev. B **79**, 155409 (2009).

[19] R. A. Sepkhanov, Y. B. Bazaliy, and C. W. J. Beenakker, Phys. Rev. A **75**, 063813 (2007).

[20] M. Plihal, A. Shambrook, and A. A. Maradudin, Opt. Commun. **80**, 199 (1991).

[21] M. Plihal and A. A. Maradudin, Phys. Rev. B **44**, 8565 (1991).

[22] D. Cassagne, C. Jouanin, and D. Bertho, Phys. Rev. B **52**, R2217 (1995); **53**, 7134 (1996); Appl. Phys. Lett. **70**, 289 (1997).

[23] F. Gadot, A. Chelnokov, A. D. Lustrac, P. Crozat, J.-M. Lourtioz, D. Cassagne, and C. Jouanin, Appl. Phys. Lett. **71**, 1780 (1997).

[24] L. Martinez, A. Garcia-Martin, and P. Postigo, Opt. Express **12**, 5684 (2004).

[25] K. Busch, G. von Freymann, S. Linden, S. Mingaleev, L. Tkeshelashvili, and M. Wegener, Phys. Reports **444**, 101 (2007).

[26] S. Raghu and F. D. M. Haldane, Phys. Rev. A **78**, 033834 (2008).

[27] M. Diem, T. Koschny, and C. M. Soukoulis, Physica B **405**, 2990 (2010).

[28] X. Zhang, Phys. Rev. Lett. **100**, 113903 (2008).

[29] Q. Liang, Y. Yan, and J. Dong, Opt. Lett. **36**, 2513 (2011).

[30] F. Dreisow, M. Heinrich, R. Keil, A. Tünnermann, S. Nolte, S. Longhi, and A. Szameit, Phys. Rev. Lett. **105**, 143902 (2010).

[31] T. Ando, T. Nakanishi, and R. Saito, J. Phys. Soc. Jpn. **67**, 2857 (1998).

[32] K. Y. Bliokh, Phys. Lett. A **344**, 127 (2005).

[33] R. Sepkhanov, A. Ossipov, and C. W. J. Beenakker, Eur. Phys. Lett. **85**, 14005 (2009).

[34] O. Peleg, G. Bartal, B. Freedman, O. Manela, M. Segev, and D. N. Christodoulides, Phys. Rev. Lett. **98**, 103901 (2007).

[35] M. Rechtsman, Y. Plotnik, D. Song, M. Heinrich, J. M. Zeuner, S. Nolte, N. Malkova, J. Xu, A. Szameit, Z. Chen, and M. Segev, arXiv:1210.5361.

[36] M. C. Rechtsman, Y. Plotnik, J. M. Zeuner, A. Szameit, and M. Segev, arXiv:1211.5683.

[37] X. Huang, Y. Lai, Z. H. Hang, H. Zheng, and C. T. Chan, Nat. Mater. **10**, 582 (2011).

[38] K. Sakoda and H-F. Zhou, Opt. Express **18**, 27371 (2010); **19**, 13899 (2011); K. Sakoda, *ibid.* **20**, 3898 (2012) **20**, 9925 (2012); **20**, 25181 (2012); J. Opt. Soc. Am. B **29**, 2770 (2012).

[39] S. Matsuzawa, K. Sato, Y. Inoue, and T. Nomura, IEICE Trans. Electron. E **89-C**, 1337 (2006).

[40] I. S. Nefedov and S. A. Tretyakov, Phys. Rev. E **66**, 036611 (2002).

[41] L. Wu, S. He, and L. Shen, Phys. Rev. B **67**, 235103 (2003).

[42] D. Bria, B. Djafari-Rouhani, A. Akjouj, L. Dobrzynski, J. P. Vigneron, E. H. ElBoudouti, and A. Nougaoui, Phys. Rev. E **69**, 066613 (2004).

[43] M. Tashima and N. Hatano, arXiv:1306.0297.

[44] M. Katsnelson, K. S. Novoselov, and A. Geim, Nat. Phys. **2**, 620 (2006).

[45] V. Cheianov, V. Fal'ko, and B. Altshuler, Science **315**, 1252 (2007).

[46] J. B. Pendry, Phys. Rev. Lett. **85**, 3966 (2000).

[47] A. Young and P. Kim, Nat. Phys. **5**, 222 (2009).

[48] Y. P. Bliokh, V. Freilikher, and F. Nori, Phys. Rev. B **81**, 075410 (2010).

[49] P. E. Allain and J. N. Fuchs, Eur. Phys. J. B **83**, 301 (2011).

[50] P. Yeh, A. Yariv,.C.-S. Hong, J. Opt. Soc. Am. **97**, 423 (1977).

[51] M. V. Berry and M. R. Jeffrey, Prog. Opt. **50**, 13 (2007).

[52] J. Li, L. Zhou, C. T. Chan, and P. Sheng, Phys. Rev. Lett. **90**, 083901 (2003).

[53] K. Artmann, Ann. Phys. Lpz. **2**, 87 (1948).

[54] M. G. Silveirinha and N. Engheta, Phys. Rev. Lett. **97**, 157403 (2006).

[55] N. C. Panoiu, R. M. Osgood, Jr., S. Zhang, and S. R. J. Brueck, J. Opt. Soc. Am. B **23**, 507 (2006).

[56] S. Feng, Phys. Rev. Lett. **108**, 193904 (2012).

[57] S. Kocaman, M. S. Aras, P. Hsieh, J. F. McMillan, C. G. Biris, N. C. Panoiu, M. B. Yu, D. L. Kwong, A. Stein, and W. Wong, Nat. Photonics **5**, 499 (2011).

[58] A. Mandatori, C. Sibilia, M. Bertolotti, S. Zhukovsky, J. W. Haus, and M. Scalora, Phys. Rev. B **70**, 165107 (2004).

[59] B. Thaller, arXiv:quant-ph/0409079.